

电阻点焊接头外观缺陷的诊断模型

张鹏贤^{1,2}, 张志芬^{1,2}, 陈剑虹^{1,2}, 王晓娥¹

(1. 兰州理工大学 有色金属合金教育部重点实验室, 兰州 730050)

2. 兰州理工大学 甘肃省有色金属新材料省部共建国家重点实验室, 兰州 730050)

摘要: 电阻点焊过程中的喷溅、电极头粘损等现象, 是导致其接头外观质量不合格的主要因素。以获取的点焊接头表面数字图像为信息源, 通过对发生喷溅和粘损情况下的图像分析, 提取了焊点图像的周长 L 、面积 S_0 、伸长率 A 和致密度 C 等作为反映图像特征的特征参量, 研究了这 4 个参量随焊接工艺参数变化的规律, 选取了 L 、 S_0 及 A 作为判识其外观缺陷的特征参量, 建立了基于支持向量机 (SVM, support vector machine) 的外观缺陷评判模型。结果表明, 该评判模型可实现对发生了外喷溅、粘损的接头外观缺陷的判识, 其准确率可达 96.67%。

关键词: 电阻点焊; 图像信息; 特征参量; 模式识别

中图分类号: TG115.28 文献标识码: A 文章编号: 0253-360X(2011)04-0005-04



张鹏贤

0 序 言

电阻点焊以其加热集中、易于实现自动化的优点被广泛应用于航空、航天、汽车等制造行业。但由于其焊接过程是热—机械联合作用过程, 易受网压波动、电极头磨损、工件表面状态等因素的干扰, 接头中难免会出现一些缺陷, 如喷溅、粘损、烧穿以及裂纹等。其中焊点表面的缺陷不仅影响着焊点的外观, 有时甚至会对接头质量、焊件的使用性能产生较大的影响。表面喷溅是由于热量输入速率过大, 熔化核心长大过度, 从而冲破塑性环在轴向冲破板表面而形成的, 其产生的疤痕影响焊件的耐腐蚀及疲劳性能。粘损是电极头与工件表面长时间相粘, 造成电极头的严重磨损, 寿命大大降低, 该缺陷在影响焊点外观质量的同时, 还会影响接头的抗腐蚀性能^[1]。

数字图像作为一种信息源可用于对焊接过程稳定性和质量进行辨识。Gang Wang 等人^[2] 基于焊缝射线图像所提取的数字特征值, 借助神经网络分类器, 实现了对焊接缺陷的分类。王克鸿等人^[3] 以图像灰度均值和标准差为特征值, 研究了 MAG 焊熔池视觉图像与焊接过程稳定性的关系。针对喷溅、粘损对点焊接头外观质量的影响, 提出了一种基于

点焊接头表面数字图像作为信息源, 建立人工神经网络诊断模型, 实现点焊接头外观质量缺陷智能判识的方法。

1 焊点表面图像的获取

图 1 为焊接过程发生了喷溅、粘损的焊点以及

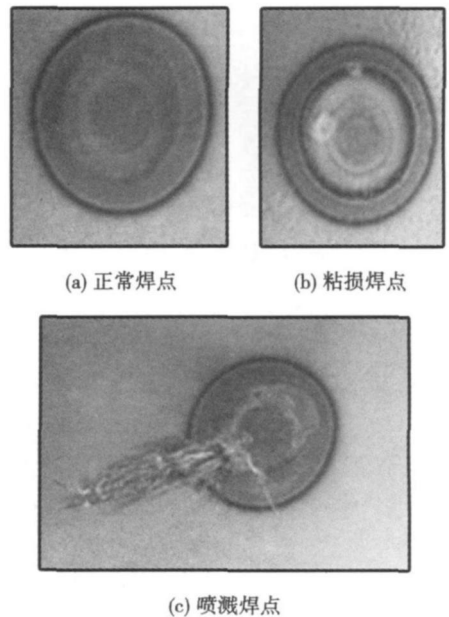


图 1 缺陷焊点与正常焊点的对比

Fig. 1 Comparison between defective spots and normal spots

收稿日期: 2009-12-04

基金项目: 国家自然科学基金资助项目 (50275028); 兰州理工大学科研基金资助项目 (h0901005)

正常焊点的表面数字图像。

试验采用唐山松下 YF-0201 乙型交流电阻点焊机, 选取工作端面直径为 6 mm 的球面电极头, 试板采用 1.0 mm 厚, 长、宽分别为 100 和 30 mm 的低碳钢, 以搭接的方式进行了点焊试验。焊后采用自行搭建的图像采集系统获取其焊点表面图像^[4], 并采用 Matlab 软件对数字图像进行了灰度化和均衡化预处理。

与正常焊点和粘损焊点近似圆形的规则形貌相比, 喷溅焊点由于外环区有明显的树枝状金属溢出物, 使其轮廓复杂, 整体线条偏长。而粘损焊点与正常焊点相比, 形态上虽并无明显差别, 但中心区域的亮度存在明显差别。正常焊点在温度场的作用下, 整体色调基本均匀, 经灰度化处理后, 其亮度较深。粘损焊点由于与电极头长时间相粘, 中心区域未发生表面氧化, 经灰度化后的该区域亮度较浅。

2 图像特征参量的提取

针对焊点表面图像, 采用阈值法对其图像进行分割后获得其二值图像^[5]。图 2 a 为焊点灰度图像对应的图像直方图, 由两个波峰和一个波谷组成。图 2 b 所示为焊点的灰度图像。灰度阈值较小的波峰是由图像中颜色较深处接头的像素点统计所得, 另一个波峰是由母材的像素点统计所得, 因此波谷为母材和焊点的临界点。故选取直方图中的波谷值作为图像分割的阈值。

根据焊点图像的特征, 尝试选用大津法 (OT-

SU) 和迭代法从直方图中自动获取波谷点对应的阈值^[6]。通过多次分割图像试验发现, 当第一个波峰值超出直方图统计范围时, 大津法无法得到真实的阈值, 而采用迭代法则可以稳定地提取波谷值作为阈值获得较满意的图像分割结果。图 2 c 所示为采用迭代法自动提取阈值对图像进行分割的结果, 该二值图像的阈值为 140.74。

图像特征是指图像中可用作标志的属性, 包括形态特征、几何特征、颜色特征、纹理特征以及统计特征。针对焊点表面二值图像, 提取其周长 L 来反映焊点的几何特征, 提取其面积 S_0 来反映焊点的颜色特征, 提取其致密度 C 及伸长率 A 来反映焊点的形态特征, 则



$$L = N_e + \sqrt{2}N_o \quad (1)$$

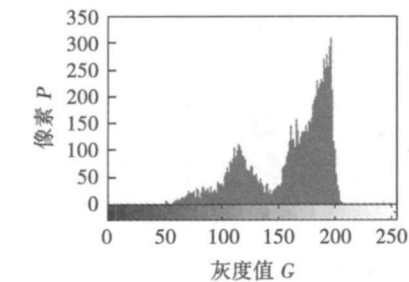
$$C = \frac{L \times L}{4\pi S_0} \quad (2)$$

$$A = \frac{\min(a, b)}{\max(a, b)} \quad (3)$$

式中: L 为周长, 计算采用 8 方向链码法^[7]; N_e 和 N_o 分别为 8 方向边界链码中走偶数步与走奇数步的数目; C 为致密度; S_0 表示二值面积, 为二值图像中所有白色区域的像素点统计值, 如表 1 所示; A 为断后伸长率, 表示图像最小外接矩形的长 a 和宽 b 中较小值与较大值的比值, 图 3 表达了焊点的 A 值提取过程。

表 1 焊点图像特征参数 S_0 的提取

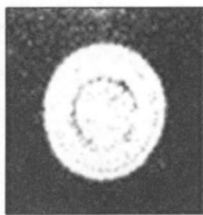
Table 1 Extraction of characteristic parameter S_0		
特征参数	正常焊点	粘损焊点
二值图像		
二值面积 S_0 (像素)	4.61×10^5	3.35×10^5



(a) 焊点灰度图像直方图



(b) 焊点灰度图像



(c) 焊点二值图像

图 2 焊点图像的二值化

FIG. 2 Binarization of joints image

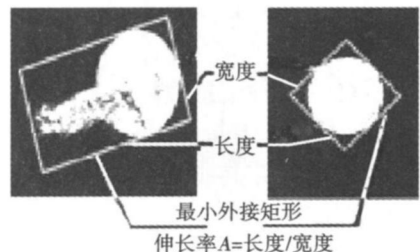


图 3 特征参量 A 的提取

Fig. 3 Extraction of characteristic parameter A

焊点表面图像的几何特征、颜色特征及形态特征与焊接工艺参数密切相关。随焊接工艺参数的不

同, 焊点表面图像的几何、形态等特征有显著的变化. 图 4 为各特征参数随焊接工艺参数变化的三维平面图. 图中每个离散点对应的是一定工艺参数下获取的焊点表面图像的特征参数. 由离散点构成的平面反映了各特征参数随工艺参数变化的趋势. 图 4^{a, b}的变化趋势基本相似, 特征参数 L 和 S_0 随着焊接电流和电极压力的增大而呈单调递增趋势.

而图 4^c中的特征参数 C 鲁棒性较差, 不能很好地表征焊点的形态特征. 图 4^d中正常焊点的特征参数 A 值不随工艺参数的变化而发生渐变, 基本保持在一定的平面内, 而图 4^e中外喷溅焊点的 A 值分布在与前者不相叠加的值域范围内. 参数 L, S_0, A 能够很好地表征不同焊接工艺参数下获取的焊点表面图像特征, 可作为焊点表面质量状态的评价因子.

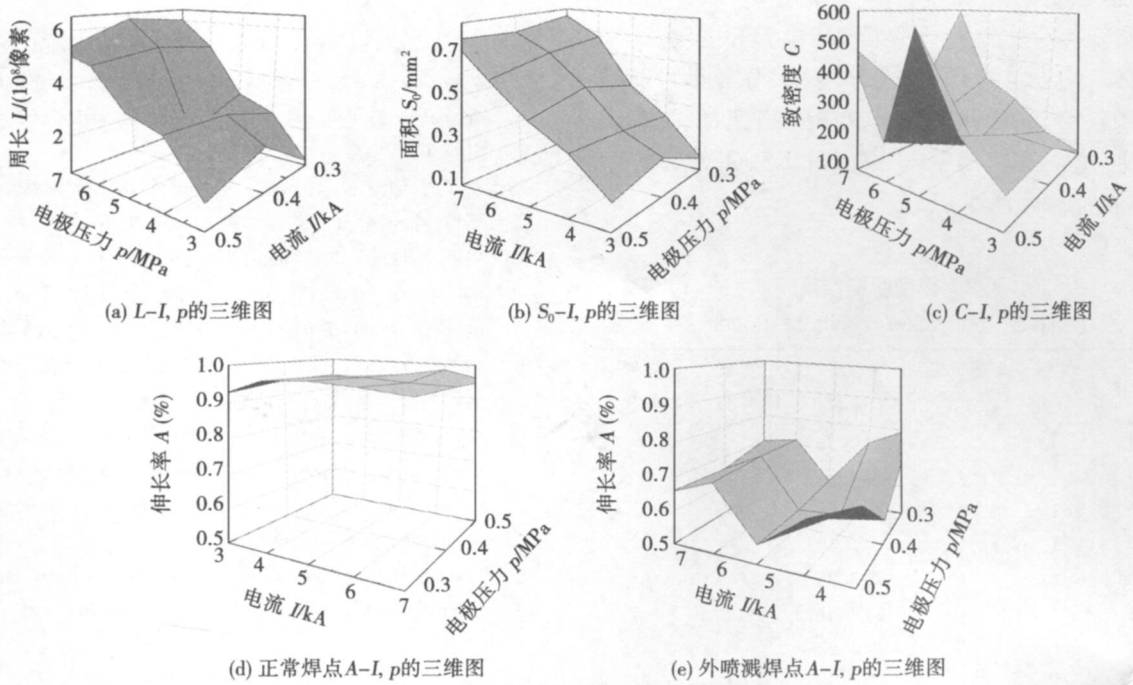


图 4 特征参数与 I, p 的三维图

Fig. 4 Three-dimensional plots of characteristic parameters and I and p

图 5 为从大量试验中所获取的正常焊点、粘损焊点和喷溅焊点的各特征值统计对比图. 焊点的分布情况表明, 不同质量状态的焊点聚集在不同的区域, 故采用 L, S_0 和 A 的值域不同分布区, 可将焊点的质量状态进行辨识.

3 SVM的评判模型

支持向量机 (SVM) 是一种基于统计学理论的模式识别方法, 在解决小样本、非线性及高维模式识别问题中表现出许多特有的优势. 其基本思想是通过定义适当的内积函数, 将训练数据从输入空间非线性地映射到一个更高维的空间里, 使得样本在该空间内线性可分, 之后求取最优线性分类面. SVM 的性能主要受核参数和误差惩罚因子 C_1 的影响. 惩罚因子 C_1 用于确定数据子空间中置信范围和经验风险的比例, 通过调整特征空间中经验误差水平来影响学习机的推广能力^[8].

以粘损、喷溅以及正常点焊接头的表面图像为信息源, 采用特征参数 L, S_0 及 A 为输入向量建立了其表面质量状态的 SVM 辨识模型. 选取同一焊接条件下的 90 组焊点, 其中正常焊点、粘损焊点以及

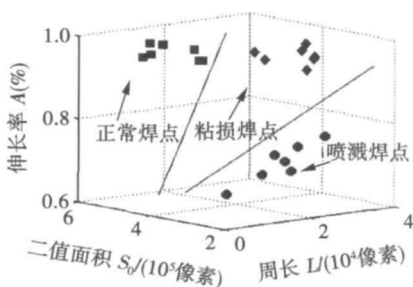


图 5 不同类焊点在 $L-S_0-A$ 三维空间中的分布

Fig. 5 Distribution of different types of joints in $L-S_0-A$ three-dimensional space

喷溅焊点分别为 30 组. 从中选取 60 组 (每类焊点 20 组) 作为分类模型的训练样本, 剩余 30 组作为测试样本. 提取每个焊点的特征值 L 、 S 及 A 构造 $[60 \times 3]$ 的输入向量和 $[60 \times 1]$ 输出向量, 其值为 0 或 1 分别对应粘损焊点、喷溅焊点和正常焊点. 采用 Matlab 下的 Libsvm 软件包, 经过优化选择最终选用 RBF 核函数, 核参数 γ 选取值为 2 惩罚因子 C 选取值为 1.

对数据进行训练得到分类模型 model 用测试样本对该分类模型进行验证, 结果显示准确率为 96.667%, 均方差为 0.133 33. 表 2 为实际验证结果, 其中仅第 28 个焊点的模型辨识结果与实测不符. 表明建立的 SVM 诊断模型可以从正常焊点中识别出粘损和喷溅类焊点.

表 2 模型验证结果

Table 2 Validation results of model

测试 样本	实测 分类	SVM 输出	测试 样本	实测 分类	SVM 输出
焊点 1	1	1	焊点 16	0	0
焊点 2	1	1	焊点 17	0	0
焊点 3	1	1	焊点 18	0	0
焊点 4	1	1	焊点 19	0	0
焊点 5	1	1	焊点 20	0	0
焊点 6	1	1	焊点 21	-1	-1
焊点 7	1	1	焊点 22	-1	-1
焊点 8	1	1	焊点 23	-1	-1
焊点 9	1	1	焊点 24	-1	-1
焊点 10	1	1	焊点 25	-1	-1
焊点 11	0	0	焊点 26	-1	-1
焊点 12	0	0	焊点 27	-1	-1
焊点 13	0	0	焊点 28	-1	1
焊点 14	0	0	焊点 29	-1	-1
焊点 15	0	0	焊点 30	-1	-1

4 结 论

获取的电阻点焊接头表面图像包含了丰富的质量信息, 提取的表征图像特征的参量周长 L 、面积 S

以及伸长率 A 可以作为基于焊点表面质量状态的评价因子. 基于特征参量 L 、 S 及 A 建立的 SVM 判别模型可实现对粘损和喷溅类焊点的判别.

参考文献:

- [1] Cho H S, Rhee S. Experimental study of nugget formation in resistance spot welding. J. Welding Journal, 2003, 82(4): 195-200.
- [2] Wang Gang, Liao TW. Automatic identification of different types of welding defects in radiographic images. J. Independent Non-destructive Testing and Evaluation International, 2002, 35(8): 519-528.
- [3] 王克鸿, 沈莹吉, 游秋榕, 等. 合金钢熔化极气保焊熔池灰度图像特征试验[J]. 焊接学报, 2007, 28(6): 73-76.
Wang K hong, Shen Yingji, You Qiurong et al. Gray image feature of molten pool in GMAW of alloy steel. J. Transactions of the China Welding Institution, 2007, 28(6): 73-76.
- [4] 张鹏贤, 陈剑虹, 杜文江. 基于焊点表面图像处理的点焊质量监测[J]. 焊接学报, 2006, 27(12): 57-63.
Zhang Pengxian, Chen Jianhong, Du Wenjiang. Quality monitoring of resistance spot welding based on image processing of welding spot surface. J. Transactions of the China Welding Institution, 2006, 27(12): 57-63.
- [5] Haralick R M, Shapiro L G. Image segmentation techniques. J. Computer Vision, Graphics and Image Processing, 1985, 29(2): 100-132.
- [6] Lee S U, Chung S Y, Park R H. A comparative study of global thresholding techniques for segmentation. J. Computer Vision, Graphics and Image Processing, 1990, 52(3): 171-190.
- [7] Gayer A, Sava A, Shikh A. Automatic recognition of welding defects in real time radiography. J. Independent Nondestructive Testing and Evaluation International, 1990, 23(3): 13-16.
- [8] Nello C, John S T. An introduction to support vector machines and other kernel based learning methods[M]. Beijing: Publishing House of Electronics Industry, 2004.

作者简介: 张鹏贤, 男, 1970 年出生, 博士, 教授. 主要从事焊接过程及其自动化、焊接质量控制等方面的研究. 发表论文 20 余篇.
Email: pengxian@163.com

MAIN TOPICS ABSTRACTS & KEY WORDS

Volume effect on shear strength of SnAgCu lead-free solder joints WANG Chunqing WANG Xuelin TIAN Yanhong (State Key Laboratory of Advanced Welding Production Technology Harbin Institute of Technology Harbin 150001 China). P1—4

Abstract SnAg0.5Cu lead-free solder joints of different sizes in the range of 200 μ m to 600 μ m were multi-reflowed and aged and then the shear strength of those solder joints were tested by the micro force tester DAGE4000. The effect of solder volume differences on the shear strength of solder joints was investigated. The results indicated that the shear strength of SnAgCu lead-free solder joints decreased with the increasing of the solder joint volume showing an apparent volume effect. The effect of aging time and reflow times on the shear strength of solder joints with different sizes were also discussed and scanning electron microscopy (SEM) was used to analyze the morphology of shear fracture and the failure mechanism of solder joints were discussed.

Key words lead-free solder joints shear strength volume effect aging multi-reflow

A diagnosis model for appearance defects of joints in RSW ZHANG Pengxiang², ZHANG Zhifeng², CHEN Jianhong², WANG Xiaod¹ (1. Key Laboratory of Non-ferrous Metal Alloys The Ministry of Education Lanzhou University of Technology Lanzhou 730050 China; 2. State Key Laboratory of Gansu Advanced Non-ferrous Metal Materials Lanzhou University of Technology Lanzhou 730050 China). P5—8

Abstract The weld metal expulsion and sticking electrode are the main factors which cause the occurrence of sub-standard appearance quality of joints in resistance spot welding. The digital images obtained from the appearance of welding joints were used as sources of information. First through the analysis of images in which expulsion and sticking occurred during the welding process the perimeter L , area S_0 , elongation A and density C were selected as the parameters to reflect the characteristic of the binary image of the joints. Second the law between the four parameters and welding parameters was revealed based on a lot of experiments. The three parameters of L , S_0 and A were extracted as the characteristic parameters to identify appearance defects of the joints. On the basis an evaluation model was established for the appearance defects of the joints based on support vector machine. At last the actual verification results showed that the evaluation model can diagnose the appearance defects caused by expulsion and sticking electrode and its accuracy can reach up to 96.67%.

Key words resistance spot welding image information characteristic parameters pattern recognition

Effect of ultrasonic frequency arc on microstructures of joint

in plasma arc welding of SiC_p/Al MMCs LEI Yuqiang², XUE Houli, HU Wenxiang, LIU Zhenzhen, YAN Jiuchun² (1. School of Material Science and Engineering Jiangsu University Zhenjiang 212013 China; 2. State Key Laboratory of Advanced Welding Production Technology Harbin Institute of Technology Harbin 150001 China). P9—12

Abstract The isolated coupling device designed according to the principles of high-pass filter is used to link the AC arc welding power and high-frequency excitation source in order to excite arc ultrasonic by modulating the alternating plasma arc. By adding Al₅Ti₅Si as filling material the effect of alternating current arc ultrasonic frequency on the microstructures of joint of $SiC_p/6061Al$ MMCs in plasma arc in-situ weld-alloying welding is investigated. By comparing the different weld microstructures under different frequencies (0, 30, 40, 50 and 60 kHz), metallographic analyses show that the morphology of Al₃Ti can be improved from a long strip into intermittent short rod-like new particle reinforced phase (AN-TN) is increased and more evenly distributed. Intragranular segregation of Si-rich phase also is significantly reduced with the frequency increase.

Key words alternating current arc ultrasonic $SiC_p/6061Al$ MMCs new reinforced composites in-situ welding

FeNi-based amorphous coatings fabricated by laser and annealing performance ZHANG Peifei, LI Zhuguo, YAO Chengwu, YU Zhishui, YAN Hua (1. School of Materials Engineering Shanghai University of Engineering Science Shanghai 201620 China; 2. Shanghai Key Laboratory of Material Laser Processing and Modification Shanghai Jiaotong University Shanghai 200240 China). P13—16

Abstract FeNi-based amorphous coating was prepared by laser cladding on the mild steel with a 15 kW continuous CO₂ laser. The phases, microstructure and the effect of addition elements on forming ability of the amorphous coatings were studied by using X-ray diffractometer and scanning electron microscope. The results show that the addition form of the ferroniobium is better than that of the pure niobium powder during the synthesis of the amorphous coating. The addition of ferroniobium can restrain the generation of the crystalline grains such as Ni₂Si and Ni₂B. The microhardness of the coating increases after annealing at 500 °C, declines at 600 °C, increases at 700 °C and 800 °C and declines at 900 °C.

Key words laser cladding FeNi-based amorphous coating

A weld robot off-line programming system integrated with virtual structured-light sensor GONG Yefei, LI Xinde, DAI Xianzhong, CHENG Xianggen (Key Laboratory of Measurement and Control of Complex Systems of Engineering Ministry of Education Southeast University Nanjing 210096 China).